

Supplementary Materials: Ultrafast X-ray Diffraction Study of a Shock-Compressed Iron Meteorite above 100 GPa

Sabrina Tecklenburg, Roberto Colina-Ruiz, Sovannndara Hok, Cynthia Bolme, Eric Galtier, Eduardo Granados, Akel Hashim, Hae Ja Lee, Sébastien Merkel, Benjamin Morrow, Bob Nagler, Kyle Ramos, Dylan Rittman, Richard Walroth, Wendy L. Mao and Arianna Gleason *

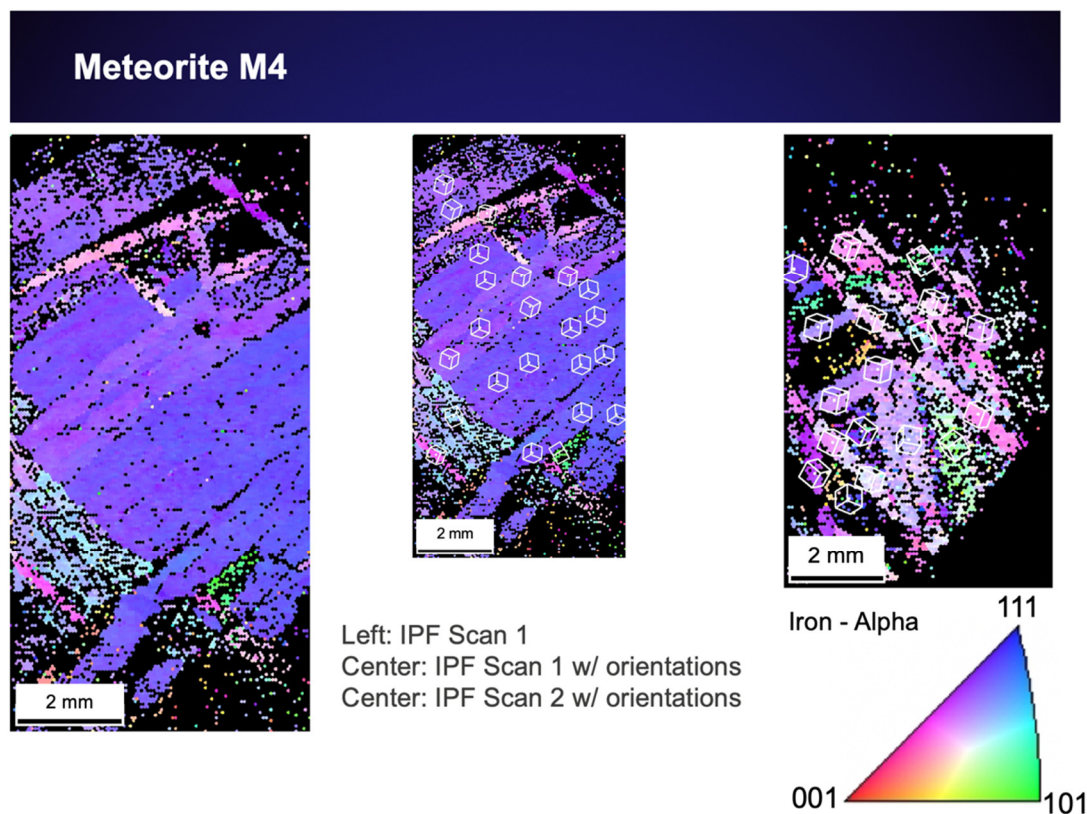


Figure S1. Electron backscatter diffraction (EBSD) image for a Gibeon meteorite sample, M4, with inverse pole figure (IPF) scans. The stereographic crystal orientation map shows the color code of bcc Fe-Ni. The orientations identified here are similar to those previously reported [1].

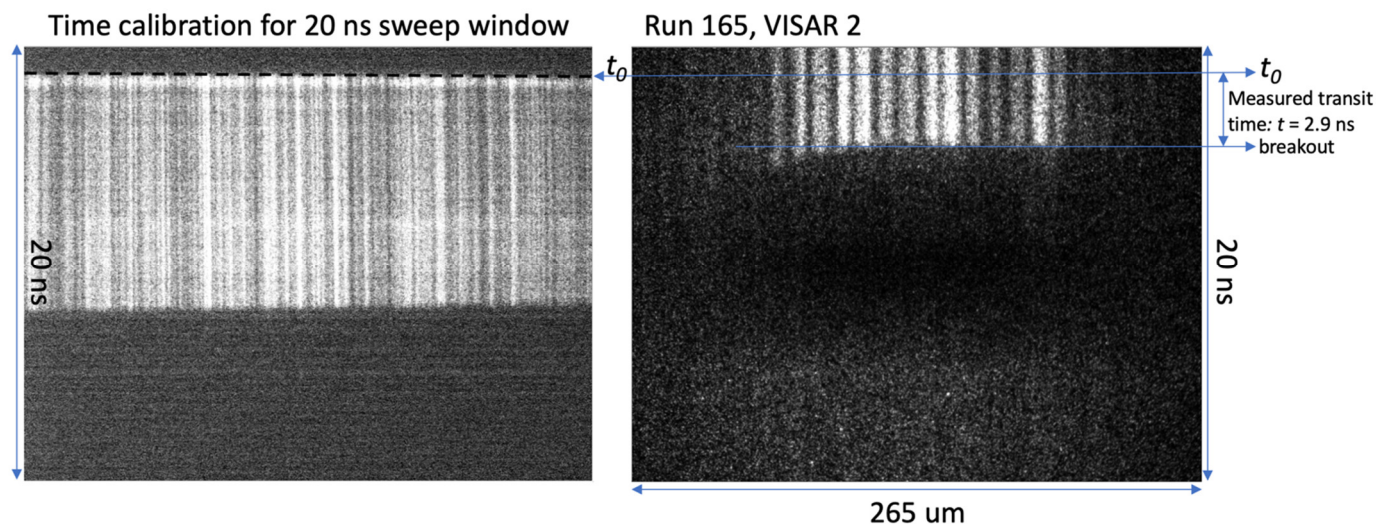


Figure S2. Representative VISAR data. **(Left)** Optical laser timing image to demark t_0 of the optical drive laser arrival on the sweep window. **(Right)** Velocity interferometer for any reflector (VISAR) [2] record from Run 165. Here we use a dual interferometric setup with two individual interferometers each with a unique delay leg set by a specific etalon thickness in the optical path to record the data. The difference in etalon thickness provides a way to differentiate between the 2π phase wraps in the velocimetry records. As a representative record, we show data from the 2nd interferometer, deemed VISAR2, Run 165. Target design did not include a lithium fluoride (LiF) window to enable quality velocimetry data; therefore, we can only extract transit time information for this study. A 20 ns sweep window had a timing offset of 5 ns applied, such that the total transit time through the target stack was the measured time of $2.9 + 5 \text{ ns} = 7.9 \text{ ns}$. The field of view from the VISAR lens location was $265 \mu\text{m}$ on target. Calibration shots on the $54 \mu\text{m}$ of plastic, labeled CH gave a shock velocity (U_s) of $\sim 16 \text{ km/s}$ in the plastic. This provided an estimated U_s in the meteorite sample of 7.5 km/s . From [3], the estimated pressure is $130 \pm 8 \text{ GPa}$, where the error has been determined by variation in the breakout time across the sample. This pressure value is in close agreement with the XRD base pressure assessment.

Supplemental Discussion

1. Shock Release Temperature Estimate

To estimate the pressure and temperature of the partial shock release state, we examined isentropic release paths derived from previous studies. We considered post-shock temperature measurements from reflectivity and emission diagnostics from Huser et al. [4] with the Sesame tables [5] for calculated release isentropes, and temperature constraints from calculated thermodynamic and equation-of-state parameter optimization for the pressure–temperature phase diagram [6]. We approximated the release isentrope trend as being a linear change in temperature from a peak pressure state to zero pressure. This approximation provides a rough guide for location in the pressure–temperature phase diagram for our late time delay XRD. The range in slopes of the release isentropes, as plotted in a pressure–temperature phase diagram for Fe, varied from 20 K/GPa at $200\text{--}100 \text{ GPa}$ down to $\sim 12 \text{ K/GPa}$ at $100\text{--}50 \text{ GPa}$ to $\sim 8 \text{ K/GPa}$ or lower at 25 GPa . Using these partial shock release slopes as guides for our data release from peak pressures of 85 and 113 GPa , we obtained constraints on the temperature of 650 ± 130 and $1150 \pm 230 \text{ K}$, respectively. The uncertainties in the temperatures were 20% derived from the estimated release trend variation at lower pressures.

2. Error Analysis

Error bars were calculated by standard propagation of the estimated standard deviation (δ) of the lattice parameters a and c from the least-squares fit determination using three peaks of the hcp structure, (100), (002), and (101), as in

$$\delta_{c/a} = \left(\frac{c}{a}\right) \sqrt{\left(\frac{\delta c}{c}\right)^2 + \left(\frac{\delta a}{a}\right)^2} \quad (1)$$

In the XRD data, where we saw only two peaks, (100) and (101), there was not a way to independently or directly constrain the c lattice parameter. The c/a ratio uncertainty cannot be assessed in the same way, so we did not report an error bar, e.g., for datum at 5.32 cm³ in Figure 5.

References

1. Nowell, M.M.; Carpenter, J.O. Multi-Length Scale Characterization of the Gibeon Meteorite using Electron Backscatter Diffraction. *Micros. Today* **2007**, *15*, 6–11, doi:10.1017/s1551929500061162.
2. Barker, L.M.; Hollenbach, R.E. Interferometer technique for measuring the dynamic mechanical properties of materials. *Rev. Sci. Instrum.* **1965**, *36*, 1617–1620, doi:10.1063/1.1719405.
3. Marsh, S.P. LASL Shock Hugoniot Data; 1980, University of California Press, Berkeley, CA, USA; ISBN 0-520-04008-2.
4. Huser, G.; Koenig, M.; Benuzzi-Mounaix, A.; Henry, E.; Vinci, T.; Faral, B.; Tomasini, M.; Telaro, B.; Batani, D. Temperature and melting of laser-shocked iron releasing into an LiF window. *Phys. Plasmas* **2005**, *12*, 1–4, doi:10.1063/1.1896375.
5. SESAME, Technical Report LA-UR-92-3407, Los Alamos National Laboratory 1992.
6. Dorogokupets, P.I.; Dymshits, A.M.; Litasov, K.D.; Sokolova, T.S. Thermodynamics and Equations of State of Iron to 350 GPa and 6000 K. *Sci. Rep.* **2017**, *7*, 1–11, doi:10.1038/srep41863.